The dependence of interfacial shear strength on temperature and matrix chemistry in glass fibre epoxy composites

Ross F. Minty*, Liu Yang and James L. Thomason

University of Strathclyde, Department of Mechanical and Aerospace Engineering

*ross.f.minty@strath.ac.uk

Ross F. Minty, Liu Yang and James L. Thomason

University of Strathclyde, Department of Mechanical Engineering, 75 Montrose Street, Glasgow G1 1XJ, United Kingdom.

Abstract

The present work focuses on a fundamental investigation into the influences of the chemistry of epoxy and the testing temperature on the stress-transfer capability of the fibre-matrix interface in a glass fibre reinforced epoxy composite. We discuss how the interfacial shear strength (IFSS) is influenced by the hardener-to-resin ratio, testing temperature and fibre silane coating respectively. It was observed that the IFSS showed a significant inverse dependence on testing temperature for both silanes, with IFSS values dropping as the temperature was increased, for all ratios studied. Notably, it was shown that once the testing temperature was raised above the glass transition temperature that ratios possessing excess amine hardener had larger IFSS values. From the results presented it is hypothesized that residual radial compressive stresses at the interface are influenced by the chemistry of the matrix system and then relax away at the higher testing temperatures.

Keywords: A Glass Fibres, A Residual/internal stress, B Fibre/matrix bond, B Interface/interphase.

1. Introduction

Over the past decades there has been a rapid growth in the development and application of fibre-reinforced composite materials for use in high performance applications. Coinciding with this there has been a concerted effort to develop a better understanding of the micro-mechanical parameters that control the structure-property relationships within such composites. Composite properties result from a combination of the properties of the fibre and the matrix as well as the ability to transfer stresses across the fibre-matrix interface. Although tailoring the interfacial stress transfer capability is widely recognized as critical to optimising the performance of a composite, it has been routinely reduced to a discussion focussed on ‘adhesion’. In this context ‘adhesion’ represents a simple term for encompassing the multiple complex mechanisms that exist at the fibre-matrix interface and contribute to its strength. One accepted mechanically measurable value for quantifying fibre-matrix adhesion is the apparent interfacial shear strength (IFSS).

Discussions about the composite interface have primarily focussed on the chemistry of the matrix system and fibre surface coating, to ensure the optimum formation of chemical bonds [1–8]. Extensive studies of

fibre sizings, and specifically the use of silane coupling agents, have been undertaken in order to attempt to better understand the specific mechanisms influencing the link between the inorganic glass fibre and the organic polymer matrix system [9–13]. However, a number of authors have also commented on the potential role of shrinkage stresses contributing to the stress transfer capability of the interface [14–22]. It has been suggested that residual radial compressive stresses at the interface may contribute significantly to the IFSS. Thermal radial compressive stresses can form during the cooling process due to differences in the thermal expansion coefficients of the matrix polymer and the reinforcement fibre. Thermosetting matrices also undergo volume change during polymerisation, known as cure shrinkage. Due to the increase of the glass transition temperature (T_g) as the thermoset matrix reacts and shrinks it is possible for some level of this cure shrinkage to be 'frozen' into the system, creating additional residual stresses at the interface [15,23]. Hence if the IFSS testing temperature is raised above the matrix T_g then these residual stresses can potentially undergo stress relaxation, decreasing IFSS. This was shown to occur by Thomason [15]. Despite this there is still a significant body of opinion that holds that even if residual stresses formed at the interface do contribute to the stress transfer capability, then chemistry and chemical reactions must still play a direct role in determining the IFSS [20,23–26].

Our previous studies have shown that the testing temperature does significantly influence the IFSS value [14,15]. This was attributed to the existence of the residual stresses at the interface, although the role of matrix chemistry in forming these stresses was not studied. We previously reported on the influence of the amine (hardener)-to-epoxy (resin) ratio (H/R) of an epoxy system on several thermomechanical properties closely linked to the strength of the interface, such as the T_g, linear coefficient of thermal expansion (LCTE) and storage modulus [27]. It was found that all properties were distinctly influenced by the chemistry of the matrix system, with optimum performance occurring around the stoichiometric value. The H/R ratio was also shown to distinctly influence the IFSS with clear correlation shown between the IFSS value and the T_g of the matrix. It was shown that the changes in thermomechanical properties influenced the contribution of the thermal residual stresses at the interface as the H/R ratio deviated from the stoichiometric value. However, this value only represented about 20% of the final IFSS value. It has been suggested that cure shrinkage stresses could potentially contribute much more to the IFSS value [23] and vary with the H/R ratio [28]. Additionally, fibre surface coatings have long been associated with increasing adhesion between the reinforcing fibre and the polymer matrix, particularly

silane coupling agents [10–13,29]. Yet the potential difference these coatings may have on the adhesion with a rubbery polymer above T_g has never been thoroughly investigated. We have therefore studied how the combination of testing temperature, H/R ratio and silane coating are interrelated to the stress transfer capability of the interface.

2. Experimental

2.1 Materials

Single boron-free E-glass fibres, coated with γ-aminopropyltriethoxysilane (APS), and glycidoxypropyltrimethoxysilane (GPS), were taken from larger rovings supplied by Owens Corning. The nominal tex was 1200 g/km and the average diameter was 17.5 μm for both. Araldite® 506 epoxy resin and triethylenetetramine (TETA) were purchased from Sigma-Aldrich and used as received.

2.2 Microbond sample preparation

The stoichiometric ratio for the system was calculated as 12.0% TETA, equating to a H/R ratio of 1.0. For the APS samples the hardener-to-epoxy ratios varied from 6.8% TETA up to 22.2% TETA, equating to H/R ratios ranging from 0.53 to 2.08. For the epoxy silane (GPS) samples three ratios were studied: 7%, 12.2% and 21.9%, equating to H/R ratios of 0.55, 1.01 and 2.05 respectively. The resin mixtures, with different H/R values, were carefully measured and mixed thoroughly before being degassed for approximated 15 minutes. Minute droplets of the resin system were then applied to a single glass fibre using a thin piece of steel wire. For each resin mixture approximately 30 droplets were placed on different individual fibres before being transferred to a convection oven where they were heated to 60 °C and held isothermally for 1 hour, then further heated to 120 °C and held isothermally for 2 hours. The heating rate was 2 °C/minute for both heating ramps and the samples were left to cool down in the oven overnight. Prior to testing, all samples were examined under 200x magnification using a Nikon Epiphot inverted microscope to obtain values for the fibre diameter (D_f) and the fibre length (L_E) embedded in the resin droplet.

2.3 TMA microbond technique

Development of the TMA microbond technique has been reported previously [14,15]. The technique uses a TA Q400 thermo-mechanical analyser, in combination with the cooling accessory MCA270 mounted with a film/fibre probe and microbond setup as shown in Figure 1. The droplet applied to the fibre sits on

the shearing plate which itself sits on the stationary quartz platform. The movable probe, installed in the centre of the stationary platform, then rests on the paper tab of the sample. It is this probe which applies the load during the test. The entire microbond setup is then enclosed within the TMA temperature controlled programmable oven. Each sample was initially placed under a very small pre-load of 0.005 N, with the free fibre length between the tab and epoxy droplet maintained at a constant value of 5 mm to match the samples tested in [27].

The notable difference between the TMA and Instron microbond techniques relates to how each technique loads the sample. The Instron technique [27] is carried out by measuring the load generated during the displacement of a droplet at a constant strain rate, however the TMA is unable to operate in this mode. Instead, the TMA was configured to measure the sample displacement during a linear force ramp of 0.15 N/min [14,15]. The testing procedure proceeded as follows: the probe displacement was electronically zeroed and the microbond sample loaded into the shearing plate with the paper tab hanging freely below the movable probe. The movable probe was then carefully lowered onto the paper tab before the furnace was closed. The initial sample length and probe position was then recorded, with the furnace then programmed to equilibrate at the desired test temperature (ranging from 20 °C to 120 °C) with an additional three-minute isothermal segment to ensure a constant equilibrium temperature was achieved. The force ramp was then initiated at 0.15 N/min. As the test proceeded the probe displacement would increase and be recorded until a successful de-bond occurred. A typical result obtained from a TMA-microbond test is plotted as a force–displacement curve in Figure 2. The major difference in the plots occurs after de-bonding. Due to the TMA continuing the force ramp after the successful de-bond, there is a rapid downward displacement of the de-bonded fibre. As such, no observations can be made on the friction region that occurs after the de-bonding process [14]. This maximum force value (F_{max}), along with the measured fibre diameter (D_f) and embedded length (L_e), was used to calculate the apparent IFSS value using Equation 1.

$$\tau_{app} = \frac{F_{max}}{\pi D_f L_e} \quad (1)$$

All tests were conducted under a nitrogen flow of 50 ml/min with approximately 30 samples per ratio tested.

3. Results and discussion

3.1 IFSS dependence on H/R ratio and testing temperature

Figure 3 shows a comparison between the TMA microbond results at 20 °C and the previous published data collected using the Instron microbond technique [27] for H/R = 1.22. It can be seen that the results collected using the TMA technique correlate well with the results collected using normal microbond testing. This indicates the microbond test carried out with our TMA and Instron setup is highly consistent in terms of obtaining IFSS. Figure 4 shows a comparison between the different testing temperatures for H/R = 1.04. We can see that as the testing temperature was increased, the max force of the microbond samples decreased, with a notable drop once the temperature was raised above the T_g value of 87.3 °C found previously in [27]. It must be noted that this value represented the peak T_g value measured in [27] which occurred at H/R ≈ 1.2, with the T_g subsequently shown to decrease as H/R ratio deviated from that value. Figures 5 and 6 shows plots where the testing temperature was maintained at constant values of 50 °C and 120 °C respectively whilst the H/R ratio of the matrix system was altered. Figure 5 shows that at 50 °C there is a degree of variation observed in the debonding behaviour of the microdroplets when changing the H/R ratio, with the degree of scatter for H/R = 2.08 observed to be larger than that of the other two ratios. For Figure 6, given the T_g value of 87.3 °C [27], 120 °C would represent a temperature that is well above the residual stress-free temperature (i.e. T_g), thus the changes observed would be thought to mainly reflect the effect of the H/R ratio on the degree of chemical bonding. Overall, it can be seen that at 120 °C the effect of changing the matrix chemistry appears greater than at 50 °C. This suggests that the importance of the matrix chemistry to the magnitude of the IFSS may be greater above T_g. It can also be seen that the plot shown in Figure 4 does show some correlation with that shown in Figure 6, with both possessing a notable point of transition.

Figure 7 presents the IFSS values versus all the testing temperatures studied, with the results representing the average of individual samples. It is indicated that the IFSS value decreased as the testing temperature was increased for all ratios, with H/R =1.04 initially exhibiting the largest IFSS values for temperatures ≤ 70 °C. A notable gap between H/R >> 1 and H/R ≈ 1 can be seen at 120 °C. The observed gradient of transition appears to occur differently depending on the specifics of the matrix chemistry, with ratios where H/R ≤ 1 appearing to lose performance sharply once above 70 °C whilst ratios where H/R > 1 appear to be less influenced above this temperature.

Figure 8 summarises the IFSS values versus all the testing temperatures and the H/R ratios of the sample respectively. The observations from Figure 7 regarding the variation in the gradient of transition with the H/R ratio are further highlighted in Figure 8. It can be seen that for temperatures below 70 °C, optimised performance occurs around the stoichiometric value (H/R = 1), but > 70 °C the IFSS value increases as more amine hardener was added to the system. Overall, the data in both Figures convey a clear dependence of the IFSS on both the chemistry of the matrix system and the testing temperature.

The data shown in Figures 7 and 8 can also be plotted as a function of ΔT as shown in Figure 9, where $\Delta T = T_t - T_g$, with T_t representing the testing temperature. Again, using values previously reported for matrix T_g [27] we can see that for the more extreme ratios of H/R = 0.53 and H/R = 2.08 the most significant changes in the values measured during the study occur at ΔT values > 0, where the polymer in theory would be in a rubbery state. Again, the gradient of the IFSS decline is clearly different for the H/R = 2.08 ratio where the step transition appears notably reduced.

A comparable series of IFSS tests as a function of temperature and a reduced number of H/R values was conducted using the GPS coated fibres. Figure 10 shows the IFSS plotted against the testing temperature for the H/R ratios studied. Overall, the plot shows a similar correlation to that shown in Figure 7, with the IFSS value decreasing as the testing temperature was increased. Once again, the maximum IFSS value was achieved, (44 MPa), at room temperature at H/R ≈ 1, however this was found to be lower than the equivalent IFSS value (49.1 MPa) recorded for the APS fibre under those conditions.

As with the APS fibres, it can be seen that at temperatures > 80 °C, the ratio where H/R >> 1 retained a higher level of IFSS, with performance at 120 °C appearing comparable to the results shown in Figure 7. One difference between the results shown in Figures 7 and 10 appears to be in the step transition of the IFSS values as the temperature was increased, with the relative decline in IFSS appearing smaller overall for GPS fibre samples where H/R < 1.2 compared to those for the APS fibre. For instance, for H/R ≈ 1 the overall percentage drop in IFSS goes from 25.2% at 70 °C to 69.6% at 80 °C, whilst for the GPS fibre the overall percentage drop goes from 31.5% to 57.5% for the same temperatures.

Figure 11 plots the IFSS results for the GPS coated fibres against the H/R ratio similarly to Figure 8. It can be seen again that, for temperatures up to 70 °C, the IFSS was maximum at H/R ≈ 1. However, for

temperatures > 70 °C performance increased as more amine was added to the system. Figure 12 highlights the smaller decline in IFSS previously discussed for the GPS fibre samples when compared to the APS fibre samples shown in Figure 8. Again, IFSS drops less significantly for R>>1. Since this occurred for both silanes it suggests that there may be other non-silane related factors influencing the IFSS as the testing temperature is increased and that these must be associated specifically with the differences in the matrix system amine content.

Overall, it appears that the IFSS was clearly influenced by the chemistry of the matrix system as well as the testing temperature, with performance deteriorating consistently as the temperature was increased for both silanes. The APS fibres appear to possess consistently higher IFSS values at lower temperatures, suggesting there may be a stronger link between the matrix and the amine sized fibres than for the epoxy sized fibres. This stronger link equated to an extra 4 MPa at H/R ≈ 1 ratio at room temperature. The ratios where APS fibres with H/R < 1 were shown to possess comparatively higher IFSS values at lower temperatures than for the GPS fibres, as shown in Figure 13. Whilst this may be explained through chemical bonding theory to some degree [5,30,31], it would be expected that the extra amine provided by the silane coating of the fibre surface should result in more bonds forming at the interface with the excess of reactive epoxy located within the matrix system since H/R < 1. The extra amine would also aid in the formation of the crosslink network within the matrix. Yet for the GPS fibres, the coating would provide further excess epoxy groups to the system, resulting in less bonding and weaker thermomechanical properties [27]. This may contribute to the difference in stress transfer capability observed between the APS and GPS coated fibres.

According to this hypothesis we might also expect the GPS fibres to perform better for ratios where H/R > 1 since the extra reactive epoxy groups provided by the silane coating would be expected to bond with the extra amine groups within the matrix system. This should facilitate more bonds formed and in theory larger IFSS values. Yet this does not seem to be the case, with the APS fibres consistently possessing higher IFSS values for these ratios. However, at temperatures > T_g the GPS fibres appear to perform comparably to the APS fibres when H/R > 1. It is interesting to note that the overall decrease in IFSS with temperature appears consistent for both silanes, suggesting that they are undergoing a similar transition despite the chemical differences at the fibre surface.

With IFSS values appearing similar for both silanes at 120 °C for all ratios, it suggests that the mixture chemistry of the matrix system may play a more important role than the chemistry of fibre coating in defining the stress transfer capability of the interface at this elevated temperature. This hypothesis, that the chemistry of the matrix has more influence over the IFSS value than the fibre coating, agrees with what can be seen in Figures 5 and 6 where at 120 °C the effect of changing the matrix chemistry appears greater than at 50 °C. This would suggest that adhesion mechanisms other than chemical bonding are contributing more to the drop in IFSS as shown in Figures 7 and 10, particularly when the temperature is elevated close to, or above, the matrix T_g. A potential explanation is that the residual radial compressive stresses (σ_R) formed at the interface during the curing process are being influenced by the properties of the matrix and relaxing away as the IFSS test temperature is increased.

3.2 Residual stress contribution to IFSS

On reviewing the results in Figures 7-13, it can be seen that the IFSS showed a significant inverse dependence on the testing temperature for both the APS and GPS fibres. With that in mind it would suggest that the deterioration in IFSS was due to factors other than a decrease in chemical bonding at the interface. One potential explanation is the existence of residual radial compressive stresses that may contribute significantly to the stress transfer capability of the fibre-matrix interface [14,15,23]. Several models have been proposed [16,17,20,32,33] to calculate these residual stresses with Nairn [16] having proposed a model showing significant normal stresses at the interface as shown in Equation 2. The benefit of Nairn's model is that it accounts for the effects of differences in axial and transverse fibre properties exhibited by many reinforcements.

$$\sigma_R = A_1\left(1 - \frac{b^2}{r^2}\right) \tag{2}$$

where A_1 is the result of the calculation shown in Equation 3.

$$A_1 = \begin{bmatrix} X_{11} & X_{12} \\ X_{21} & X_{22} \end{bmatrix}\begin{bmatrix} A_1 \\ A_3 \end{bmatrix} = \begin{bmatrix} (\alpha_m - \alpha_{fT})\Delta T \\ (\alpha_m - \alpha_{fL})\Delta T \end{bmatrix} \tag{3}$$

The model shown in Equation 3 represents a simplification of the composite cylinder model proposed in [16]. Nairn assumed the volume fraction of the interphase to be zero which allowed for the equation to be reduced to a two-by-two linear system. The X terms represent elements of the matrix that can be calculated if certain material properties of the fibre and matrix are known, such as modulus, Poisson's ratio, and volume fraction. These expressions are detailed in [16].

Of the variables presented, b is a function of the fibre volume ratio (V_f), r is the radius of the fibre, α is the linear coefficient of thermal expansion, ΔT represents the difference between the stress-free temperature (T_s) and the testing temperature (T_t), and f, m, L and T represent subscripts for the fibre, matrix, longitudinal and transverse respectively. From the form of Equation 3 the interfacial thermal residual stresses are directly influenced by changes in ΔT, thus we would expect the thermal residual stresses to relax away as T_t increase and surpasses T_s which itself is highly related to the T_g of the system. Our previous work [27] showed that both the T_g and LCTE of the polymer are highly influenced by the epoxy-to-hardener ratio and thus thermal residual stresses were similarly affected. Using this data in combination with a coefficient of static friction of $\mu_s = 0.6$ [12,30] allowed for the residual stress contribution to the interfacial stress transfer capability (τ_R) to be obtained using Equation 4.

$$\tau_R = \mu\sigma_R \tag{4}$$

Taking this previously published thermal residual stress data [27] and combining it with the TMA microbond data presented here allows us to plot the IFSS value for each ratio against the residual stress contribution to the interfacial stress transfer capability (τ_R). Figure 14 shows the comparison for the stoichiometric value (H/R = 1.0) whilst Figures 15 and 16 show comparable plots for ratios of H/R = 0.53 and H/R = 2.06 respectively. It can be seen that for each H/R ratio there is some level of correlation between the IFSS decrease with temperature and the relaxation of the residual stresses due to thermal shrinkage as the testing temperature was raised. However, it is also clear that the residual stresses due to thermal shrinkage could only be making a small contribution to the overall IFSS values observed in the system.

One significant difference between thermosetting and thermoplastic systems is that thermosets will undergo chemical shrinkage during the curing process due to the polymerization reaction. This cure shrinkage can result in significant volumetric changes, applying a large degree of strain to the system. Di Landro and Pegoraro [20] have previously discussed how cure shrinkage may provide the bulk of the residual stresses when compared to thermal shrinkage stresses in thermoset systems. However, any cure shrinkage that occurs before the gel point of the system can potentially relax away. This can be attributed to the low molecular weight and liquid nature of the matrix in this state. Gelation is defined as the liquid–solid transition of an epoxy resin that occurs when the average molecular weight approaches infinity. One

can reasonably assume that any strain induced by cure shrinkage will require more time to relax away as the system approaches the gel point. Thus, once the gel point is exceeded then any further cure shrinkage related residual strain will be locked into the epoxy network. As the system is cooled back through T_g the matrix modulus will increase and consequently the residual stress from the cure shrinkage strain will increase in proportion to the matrix modulus. This hypothesis fits with the relationships observed in Figures 7 and 10 where the increase in temperature would lead towards this stress potentially relaxing away. Applying this hypothesis, using our modulus data from [27] and applying an isothermal volumetric cure shrinkage value of -6% [15,23,34,35] produces the additional stress curves (marked as cure shrinkage and total shrinkage) shown in Figures 14-16. It can be seen that the residual stress contribution due to cure shrinkage appears to be significantly larger than that provided by the thermal shrinkage for each ratio. This is in agreement with the results discussed by both Thomason [15] and Jakobsen [23].

Figures 14-16 show that the residual radial compressive stresses at the interface could indeed be contributing significantly to the stress transfer capability of the interface at room temperature. The sum of the thermal and cure shrinkage contributions produces a value comparable in magnitude to that measured using the microbond technique. However, it appears that the decrease of IFSS at temperatures above the T_g cannot be due to just the residual stresses at the interface relaxing away. Specifically, at 120 °C there is still a distinct level of adhesion shown to remain between the fibre and matrix, at a point where it would have been expected that all the residual stresses have relaxed away. As discussed previously, at these higher temperatures the IFSS value appears to be dictated by the chemistry of the matrix, not the surface coating of the fibre, and scales linearly with the level of amine in the matrix system. Applying chemical theory, one would expect the IFSS value to decrease as the ratio deviated from stoichiometry, with the number of bonds across the interface decreasing and the level of crosslinking within the matrix also decreasing [36,37]. That statement would apply to a glassy state polymer and match what was shown below T_g, yet at 120 °C the epoxy matrix would be in a rubbery state, with perhaps other mechanisms governing the stress transfer capability. One hypothesis would be that hydrogen bonding within the matrix increases as more amine hardener is added to the system, leading to the observed lessened decrease in IFSS observed in Figures 7 and 10. This would occur since the excess hardener within the system would result in an abundance of reactive hydrogen atoms remaining within the matrix structure, contributing to the level of hydrogen bonding present. This would also explain the linear increase shown

in Figures 7 and 10 as the ratio was increased, with the hydrogen bonding now potentially providing a significant contribution to the adhesion remaining in the system.

Another hypothesis is that at these higher temperatures, due to the polymer now being a rubber, the nature of the debonding process is being influenced by the R ratio. D'Almeida has discussed [38–41] how epoxy matrices containing excess amine can possess greater deformation capacity than at lower H/R ratios. Thus, at these higher temperatures the higher H/R ratio matrices may be superior at maintaining the stress transfer capability at the interface whilst under load due to a better stress distribution across the droplet during the microbond test. Zhao [42] also observed that variations in the crosslink density could significantly impact the shear failure behavior in amorphous polymers. Zhao found that the ultimate stresses and the broken ratios, (the bond number to all polymer chain number ratios), increased with increasing crosslink density under shear, but that the ultimate strains decreased with increasing crosslink density. Furthermore Zhao found that when the temperature was varied, the broken ratio varied significantly due to the potential reorganization of the polymer structure [42]. These observations could partially explain the data shown in Figures 7 and 10 and why excess amine ratios perform superior to those ratios where H/R ≈ 1 and temperature > T_g. However, ratios where H/R < 1 would also possess smaller crosslink density values [36] and thus would be expected to benefit in the same manner; yet they do not. As such it could be hypothesized that although this mechanism may be contributing to the stress transfer capability of the interface, its contribution is less than other mechanisms. This, combined with the hydrogen bonding theory, may potentially explain the IFSS value trends shown at temperatures above T_g.

Analyzing Figures 14-16, it can be seen that whilst the assumptions for Nairn's model [16] appear acceptable for the stoichiometric ratio (H/R ≈ 1.0), the model appears to be less accurate for the other two ratios plotted. Specifically for H/R ≈ 1.0 it can be seen that the predicted combined contribution of the thermal and cure stresses to the interface, and subsequent relaxation away with increasing temperature, correlate well with the experimental IFSS data gathered. However, for H/R ≈ 0.5 the residual stress contribution appears to relax away before the IFSS value begins to drop drastically, whilst for H/R ≈ 2.0 the model predicts a distinctly larger IFSS value at room temperature than was measured. Both cases suggest that whilst residual stresses may contribute to the stress transfer capability of the interface, other mechanisms may contribute more for ratios off-stoichiometry. One assumption made for the models,

which may explain the extra contribution towards IFSS from residual radial stresses shown for H/R ≈ 2.0, is the use of a constant value, and 100%, of cure shrinkage in the model calculations. This does not account for the fact that some fraction of the cure shrinkage related strain would have relaxed away before the resin reached gelation. Thus, the degree of shrinkage frozen into the matrix structure would be influenced by the gel point of the system, as well as the degree of shrinkage that occurred. The level of cure shrinkage in epoxy matrices has been shown to change with different curing schedules [26,43,44] and with the influence of different H/R ratios on cure kinetics [45,46]. It can be hypothesized that a similar relationship may exist between matrix chemistry, cure shrinkage, residual interfacial stress and interfacial stress transfer capability. This hypothesis led to the investigation using a novel hot-stage microscope technique in [28] where it was found that the degree of chemical cure shrinkage increased as the H/R ratio was increased.

Taking the data produced in [28] Figures 14-16 can be adjusted accordingly to take account of the different degrees of cure shrinkage found to occur for the different H/R ratios. Figure 17 shows that the results of Nairn's model do correlate well with the measured IFSS results for the TMA microbond technique for ratios near to the stoichiometric value. Since the level of cure shrinkage measured was smaller than the original 8% assumed for Figure 14, the contribution values appear to be smaller. However, if the coefficient of static friction is slightly increased from 0.6 up to 0.75 as shown in Figure 20 then the two plots are shown to correlate to a greater degree. Another potential reason for the lack of correlation in the temperature region above T_g may be due to the assumption made between the residual stress and the gel point by the model. In reality the transition of residual stresses being "frozen-in" once the gel point is crossed may not be clear cut. Given the visco-elastic nature of the polymer (or polymerizing polymer) the "frozen-in" stress may start to build up even before the gel point, to give a more gradual increase in residual stress as observed in the IFSS data. Overall, these results would support the hypothesis that residual stresses can contribute significantly to the stress transfer capability of the interface. Figures 17 and 20 suggest that there does exist a clear link between the IFSS and the residual stress contribution.

It can be seen that the contributions predicted by the model for H/R ≈ 0.5 and H/R ≈ 2.0 again appear to correlate poorly with the results produced by the TMA microbond method. This was also the case in Figures 15 and 16, although the decrease in cure shrinkage for H/R ≈ 0.5 appears to have been impacted

the most. It can be seen that the contribution of the residual stresses to the IFSS equates to only ≈ 20 MPa maximum. Compared to the 46 MPa measured at 20 °C this would confirm that other adhesion mechanisms must be at work in order to produce this value. In addition to this, both plots show that the residual stress contribution decreases before any notable drop in IFSS occurs. For H/R ≈ 0.5 the value for IFSS drops ≈ 70 °C, while the residual stress contribution is shown to have relaxed away ≈ 50 °C. In the case of H/R ≈ 2.0, the suggested contribution at 20 °C still appears notably larger than the measured IFSS. This was also the case in the original model in Figure 16. The contribution is then shown to relax away at ≈ 60 °C while the IFSS maintains a gradual decline. Both would suggest that the residual stress contribution is not the key contributor of the complex mechanisms at work at the interface, highlighting the limits of the model currently used. Compared to the results for H/R ≈ 1.0, it appears that the contribution of the residual stresses plays a more central role in defining the value for IFSS the nearer the H/R value is to stoichiometry. Once the ratio begins to deviate from this value, the significance of the residual stresses appears to decrease. However, the apparent limits of the model are directly linked to our lack of understanding regarding the T_g of an epoxy microdroplet. This is due to the model assuming that the T_g of the droplet is the same as the bulk value measured using DSC in [27], where it was shown that the T_g could vary significantly for H/R >> 1 or << 1. It has been shown in the past by Zinck [47] that the T_g of a thin film of resin differed from that of the bulk matrix. They also suggested that this affected their microbond results. Both Thomason [48] and Bryce [49] have found that the results of the microbond test can be highly dependent on the properties of the microdroplet, with the issue of scaling being highlighted as a challenging factor when it comes to assuming T_g values that reflect the properties of the macroscale composite [48]. Given the importance of the T_g value towards the stress-free temperature T_s and the residual stress created from the cure shrinkage strain, this would provide an explanation for why the model works for H/R ≈ 1.0 but not for off-stoichiometric values. The possibility of this T_g scaling issue also being influenced by the H/R value would also explain why the results of the model decrease in correlation the further the H/R value deviates from stoichiometry. Nevertheless, it can be seen that there exists a relationship between the IFSS value, the H/R value, the testing temperature and potential residual stresses “frozen in” at the fibre-matrix interface. Further study of the T_g value of epoxy microdroplets, the effect of the H/R ratio on the scaling factor discussed in [48,49] and an investigation into the specific friction coefficient of the fibres studied would be beneficial for use in Nairn’s model used for this paper.

4. Conclusions and concluding remarks

The results presented in this paper show that the hardener-to-epoxy ratio, testing temperature and fibre silane coating can each influence the stress transfer capability of the interface in a glass fibre reinforced epoxy composite. Each hardener-to-epoxy ratio tested was shown to possess different IFSS values at each testing temperature. Below the epoxy polymer T_g, the highest IFSS values were shown to occur at the stoichiometric value, with IFSS decreasing as the ratio deviated further from this value for both types of silane coated fibres investigated. However, as the temperature was increased a transition in IFSS was observed when the testing temperature exceeded 70 °C. Whilst interfacial performance continued to decrease overall after this point, the optimum relative IFSS value was shown to improve linearly when more amine was added to the epoxy system. This was even the case when the testing temperature was raised further to 120 °C. It was shown that there was some correlation between the deterioration in IFSS and the potential relaxation of the "frozen" in residual stresses at the interface as the temperature was increased. This was shown particularly for H/R ratios close to the stoichiometric value. It was also observed that at temperatures well above T_g a small value of IFSS still existed, despite the residual stresses having likely relaxed away. It was hypothesized that an increased level of hydrogen bonding, due to the increasing amine content of the matrix system, combined with the variation in shear failure behavior of the matrix due to the differing crosslink densities, was potentially responsible for this. One practical conclusion from the results presented here is that performance of the interface in thermoset composites is strongly related to the chemistry of the polymer matrix adjacent to that interface as well as the temperature of the surrounding environment. Fibre sizings typically contain chemical reactive groups similar to the polymer matrices in their composites which may well result in unexpected local variations in the H/R ratio. Hence it is also possible that key interface properties of a glass fibre-reinforced epoxy composite may vary along the entire length of the embedded fibre. Small changes in H/R may result in small variations in the level of adhesion with minimum impact on performance. However, if the local variation from the stoichiometric value is large enough then there may be potential for a significant impact on performance of the final composite material, with the effect of this increasing with rising temperatures.

CRediT authorship contribution statement

Ross Minty: Investigation, Data curation, Formal analysis, Writing – original draft, Writing - review & editing. **Liu Yang**: Methodology, Supervision, Writing - review & editing. **James Thomason**: Conceptualization, Funding acquisition, Supervision, Writing - review & editing.

Declaration of competing interest

The authors declare that they have no known competing financial interests or personal relationships that could have appeared to influence the work reported in this paper.

Acknowledgements

The authors gratefully acknowledge the support of the Engineering and Physical Sciences Research Council (EPSRC) for funding this study.

References

[1] Broutman LJJ. Measurement of the Fiber-Polymer Matrix Interfacial Strength. Interfaces Compos ASTM STP 452 1969:27–41.

[2] Dey M, Deitzel JM, Gillespie JW, Schweiger S. Influence of sizing formulations on glass/epoxy interphase properties. Compos Part A Appl Sci Manuf 2014;63:59–67. https://doi.org/10.1016/j.compositesa.2014.04.006.

[3] Drown EK, Al Moussawi H, Drzal L. Glass fiber sizings and their role in fiber-matrix adhesion. J Adhes Sci Technol 1991;5:865–81. https://doi.org/10.1163/156856191X00260.

[4] Drzal LT, Sugiura N, Hook D. The role of chemical bonding and surface topography in adhesion between carbon fibers and epoxy matrices? Compos Interfaces 1996;4:337–54. https://doi.org/10.1163/156855497X00073.

[5] Drzal LT, Madhukar M. Fibre-matrix adhesion and its relationship to composite mechanical properties. J Mater Sci 1993;28:569–610. https://doi.org/10.1007/BF01151234.

[6] Gray RJ, Johnston CD. The effect of matrix composition on fibre/matrix interfacial bond shear strength in fibre-reinforced mortar. Cem Concr Res 1984;14:285–96. https://doi.org/10.1016/0008-8846(84)90116-9.

[7] Jones FR. A Review of Interphase Formation and Design in Fibre-Reinforced Composites. vol. 24. 2010. https://doi.org/10.1163/016942409X12579497420609.

[8] Plonka R, Mäder E, Gao SL, Bellmann C, Dutschk V, Zhandarov S. Adhesion of epoxy/glass fibre composites influenced by aging effects on sizings. Compos Part A Appl Sci Manuf 2004;35:1207–16. https://doi.org/10.1016/j.compositesa.2004.03.005.

[9] Plueddemann EP. Adhesion Through Silane Coupling Agents. J Adhes 1970;2:184–201. https://doi.org/10.1080/0021846708544592.

[10] Plueddemann EP. Reminiscing on silane coupling agents. J Adhes Sci Technol 1990;5:261–77. https://doi.org/10.1163/156856191X00350.

[11] DiBenedetto AT. Tailoring of interfaces in glass fiber reinforced polymer composites: a review. Mater Sci Eng A 2001;302:74–82. https://doi.org/10.1016/S0921-5093(00)01357-5.

[12] Debnath S, Wunder SL, McCool JI, Baran GR. Silane treatment effects on glass/resin interfacial

shear strengths. Dent Mater 2003;19:441–8. https://doi.org/10.1016/S0109-5641(02)00089-1.

[13] Kaynak C, Celikbilek C, Akovali G. Use of silane coupling agents to improve epoxy-rubber interface. Eur Polym J 2003;39:1125–32. https://doi.org/10.1016/S0014-3057(02)00381-6.

[14] Thomason JL, Yang L. Temperature dependence of the interfacial shear strength in glass-fibre polypropylene composites. Compos Sci Technol 2011;71:1600–5. https://doi.org/10.1016/j.compscitech.2011.07.006.

[15] Thomason JL, Yang L. Temperature dependence of the interfacial shear strength in glass-fibre epoxy composites. Compos Sci Technol 2014;96:7–12. https://doi.org/10.1016/j.compscitech.2014.03.009.

[16] Nairn JA. Thermoelastic analysis of residual stresses in unidirectional, high-performance composites. Polym Compos 1985;6:123–30. https://doi.org/10.1002/pc.750060211.

[17] Raghava RS. Thermal expansion of organic and inorganic matrix composites: A Review of theoretical and experimental studies. Polym Compos 1988;9:1–11. https://doi.org/10.1002/pc.750090102.

[18] Wagner HD, Nairn JA. Residual thermal stresses in three concentric transversely isotropic cylinders: application to composites containing a interphase. Compos Sci Technol 1997;57:1289–302. https://doi.org/10.1016/S0266-3538(97)00058-4.

[19] Di Landro L, Pegoraro M. Carbon fibre thermoplastic matrix adhesion. J Mater Sci 1987;22:1980–6. https://doi.org/10.1007/BF01132927.

[20] Landro L Di, Pegoraro M, Di Landro L, Pegoraro M. Evaluation of residual stresses and adhesion in polymer composites. Compos Part A Appl Sci Manuf 1996;27:847–53. https://doi.org/10.1016/1359-835X(96)00046-2.

[21] Biro DA, Pleizier G, Deslandes Y. Application of the microbond technique: Effects of hygrothermal exposure on carbon-fiber/epoxy interfaces. Compos Sci Technol 1993;46:293–301. https://doi.org/10.1016/0266-3538(93)90163-B.

[22] Zhao LG, Warrior NA, Long AC. A micromechanical study of residual stress and its effect on transverse failure in polymer-matrix composites. Int J Solids Struct 2006;43:5449–67. https://doi.org/10.1016/j.ijsolstr.2005.08.012.

[23] Jakobsen J, Jensen M, Andreasen JHH. Thermo-mechanical characterisation of in-plane properties for CSM E-glass epoxy polymer composite materials – Part 1: Thermal and chemical strain. Polym Test 2013;32:1350–7. https://doi.org/10.1016/j.polymertesting.2013.08.010.

[24] Chekanov YA, Korotkov VN, Rozenberg BA, Dhzavadyan EA, Bogdanova LM. Cure shrinkage defects in epoxy resins. Polymer (Guildf) 1995;36:2013–7. https://doi.org/10.1016/0032-3861(95)91446-E.

[25] Ismail H, Shuhelmy S, Edyham MR. The effects of a silane coupling agent on curing characteristics and mechanical properties of bamboo fibre filled natural rubber composites. Eur Polym J 2002;38:39–47. https://doi.org/10.1016/S0014-3057(01)00113-6.

[26] Ramos JA, Pagani N, Riccardi CC, Borrajo J, Goyanes SN, Mondragon I. Cure kinetics and shrinkage model for epoxy-amine systems. Polymer (Guildf) 2005;46:3323–8. https://doi.org/10.1016/j.polymer.2005.02.069.

[27] Minty RF, Yang L, Thomason JL. The influence of hardener-to-epoxy ratio on the interfacial strength in glass fibre reinforced epoxy composites. Compos Part A 2018;112:64–70. https://doi.org/10.1016/j.compositesa.2018.05.033.

[28] Minty RF, Thomason JL, Yang L, Stanley W, Roy A. Development and application of novel technique for characterising the cure shrinkage of epoxy resins. Polym Test 2019;73:316–26. https://doi.org/10.1016/j.polymertesting.2018.11.045.

[29] Thomason JL. Glass Fibre Sizings: A Review of the Scientific Literature. Blurb Inc; 2012.

[30] Vanlandingham MR, Eduljee RF, Gillespie JW, Gillespie Jr. JW. Relationships between stoichiometry, microstructure, and properties for amine-cured epoxies. J Appl Polym Sci 1999;71:699–712. https://doi.org/10.1002/(sici)1097-4628(19990131)71:5<699::aid-app4>3.0.co;2-d.

[31] D'Almeida JRM, de Menezes WG, Neves Monteiro S. Ageing of the DGEBA / TETA Epoxy System with off-Stoichiometric Compositions 2 . Experimental Methods And Materials. Mater Res 2003;6:415–20. https://doi.org/10.1590/S1516-14392003000300017.

[32] Takaku A, Arridge RGC. The effect of interfacial radial and shear stress on fibre pull-out in composite materials. J Phys D Appl Phys 1973;6:2038–47. https://doi.org/10.1088/0022-3727/6/17/310.

[33] Detassis M, Pegoretti A, Migliaresi C, Wagner HD. Experimental evaluation of residual stresses in single fibre composites by means of the fragmentation test. J Mater Sci 1996;31:2385–92. https://doi.org/10.1007/BF01152951.

[34] Li C, Potter K, Wisnom MR, Stringer G. In-situ measurement of chemical shrinkage of MY750 epoxy resin by a novel gravimetric method. Compos Sci Technol 2004;64:55–64. https://doi.org/10.1016/S0266-3538(03)00199-4.

[35] Hoa S V., Ouellette P, Ngo TD. Determination of shrinkage and modulus development of thermosetting resins. J Compos Mater 2009;43:783–803. https://doi.org/10.1177/0021998308102035.

[36] Palmese GR, McCullough RL. Effect of epoxy–amine stoichiometry on cured resin material properties. J Appl Polym Sci 1992;46:1863–73. https://doi.org/10.1002/app.1992.070461018.

[37] Levita G, De Petris S, Marchetti A, Lazzeri A. Crosslink density and fracture toughness of epoxy resins. J Mater Sci 1991;26:2348–52. https://doi.org/10.1007/BF01130180.

[38] D'Almeida JRM, Monteiro SN. The Effect of the resin/hardener ratio on the compressive behavior of an epoxy system. Polym Test 1996;15:329–39. https://doi.org/10.1016/0142-9418(95)00037-2.

[39] D'Almeida JRM, Monteiro SN. Role of the resin matrix/hardener ratio on the mechanical properties of low volume fraction epoxy composites. Adv Perform Mater 1997;4:285–95. https://doi.org/10.1023/A:1008625121464.

[40] D'Almeida JRM, Monteiro SN. The resin/hardener ratio as a processing parameter for modifying the mechanical behaviour of epoxy-matrix/glass microsphere composites. Compos Sci Technol 1998;58:1593–8. https://doi.org/10.1016/S0266-3538(97)00223-6.

[41] D'Almeida JRM, Monteiro SN. The Influence of the Amount of Hardener on the Tensile Mechanical Behavior of an Epoxy System. Polym Adv Technlogies 1998;9:216–21. https://doi.org/10.1002/(SICI)1099-1581(199803)9:3<216::AID-PAT746>3.0.CO;2-S.

[42] Zhao J, Yu P, Dong S. The influence of crosslink density on the failure behavior in amorphous polymers by molecular dynamics simulations. Materials (Basel) 2016;9. https://doi.org/10.3390/ma9040234.

[43] Shah DU, Schubel PJ. Evaluation of cure shrinkage measurement techniques for thermosetting resins. Polym Test 2010;29:629–39. https://doi.org/10.1016/j.polymertesting.2010.05.001.

[44] Khoun LL, Hubert P. Cure Shrinkage Characterization of an Epoxy Resin System by Two in Situ Measurement Methods. Polym Compos 2010;31:1603–10. https://doi.org/10.1002/pc.

[45] Karayannidou EG, Achilias DS, Sideridou ID. Cure kinetics of epoxy-amine resins used in the restoration of works of art from glass or ceramic. Eur Polym J 2006;42:3311–23. https://doi.org/10.1016/j.eurpolymj.2006.08.025.

[46] Thomason JL, Yang L, Bryce D, Minty R. An exploration of the relationship of chemical and physical parameters in the micromechanical characterisation of the apparent interfacial strength in glass fibre epoxy systems. IOP Conf Ser Mater Sci Eng 2016;139:012048. https://doi.org/10.1088/1757-899X/139/1/012048.

[47] Zinck P, Wagner HD, Salmon L, Gerard JF. Are microcomposites realistic models of the fibre / matrix interface? II . Physico-chemical approach. Polymer (Guildf) 2001;42:6641–50. https://doi.org/10.1016/S0032-3861(00)00871-5.

[48] Thomason J. An overview of some scaling issues in the sample preparation and data interpretation of the microbond test for fibre-matrix interface characterisation. Polym Test 2022;111:107591. https://doi.org/10.1016/j.polymertesting.2022.107591.

[49] Bryce D, Thomason J, Yang L. Micromechanical and spectroscopic characterisation of the curing performance of epoxy resins in the microbond test. IOP Conf. Ser. Mater. Sci. Eng., vol. 942, IOP Publishing Ltd; 2020. https://doi.org/10.1088/1757-899X/942/1/012019.

Figure Captions

Figure 1. Schematic and close up photograph of TMA-Microbond test setup [15].

Figure 2. Load/ Displacement Cure for TMA microbond test.

Figure 3. Comparison between force/displacement plots collected using the TMA microbond technique and data collected using the Instron microbond technique, amine (hardener)-to-epoxy (resin) ratio = 1.22 and testing temperature = 20 °C.

Figure 4. Comparison between force/displacement plots for amine (hardener)-to-epoxy (resin) ratio = 1.04 at different testing temperatures.

Figure 5. Comparison between force/displacement plots for different amine (hardener)-to-epoxy (resin) ratios at a testing temperature 50 °C.

Figure 6. Comparison between force/displacement plots for different amine (hardener)-to-epoxy (resin) ratios at a testing temperature 120 °C.

Figure 7. Plot of IFSS versus Testing Temperature for APS fibres.

Figure 8. Plot of IFSS versus amine (hardener)-to-epoxy (resin) ratio (H/R) for APS fibres.

Figure 9. Plot of IFSS versus ΔT, where $\Delta T = T_t - T_g$ for APS fibres.

Figure 10. Plot of IFSS versus Testing Temperature for GPS fibres.

Figure 11. Plot of IFSS versus amine (hardener)-to-epoxy (resin) ratio (H/R) for GPS fibres.

Figure 12. Plot of IFSS versus ΔT, where $\Delta T = T_t - T_g$ for GPS fibres.

Figure 13. Plot comparing results for H/R ≈ 0.5, H/R ≈ 1.0 and H/R ≈ 2.0 for both silanes studied.

Figure 14. Comparison of glass fibre epoxy IFSS with calculated residual radial stresses for an amine (hardener)-to-epoxy (resin) ratio of H/R ≈ 1.0 (the stoichiometric value).

Figure 15. Comparison of glass fibre epoxy IFSS with calculated residual radial stresses for an amine (hardener)-to-epoxy (resin) ratio of H/R ≈ 0.5.

Figure 16. Comparison of glass fibre epoxy IFSS with calculated residual radial stresses for an amine (hardener)-to-epoxy (resin) ratio of H/R ≈ 2.0.

Figure 17. Comparison of glass fibre epoxy IFSS with adjusted residual radial stresses for an amine (hardener)-to-epoxy (resin) ratio of H/R ≈ 1.0 (the stoichiometric value).

Figure 18. Comparison of glass fibre epoxy IFSS with adjusted residual radial stresses for an amine (hardener)-to-epoxy (resin) ratio of H/R ≈ 0.5.

Figure 19. Comparison of glass fibre epoxy IFSS with adjusted residual radial stresses for an amine (hardener)-to-epoxy (resin) ratio of H/R ≈ 2.0.

Figure 20. Comparison of glass fibre epoxy IFSS with adjusted residual radial stresses for an amine (hardener)-to-epoxy (resin) ratio of H/R ≈ 1.0 (the stoichiometric value) using a coefficient of static friction = 0.75.

Figures

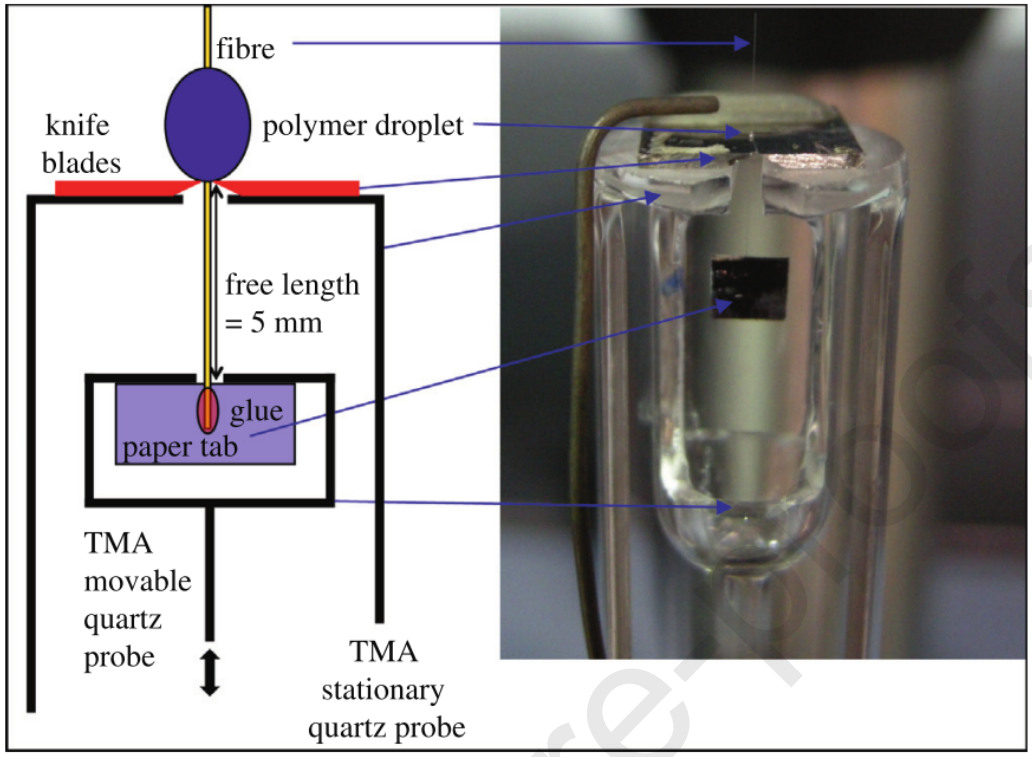

Figure 1. Schematic and close up photograph of TMA-Microbond test setup [15].

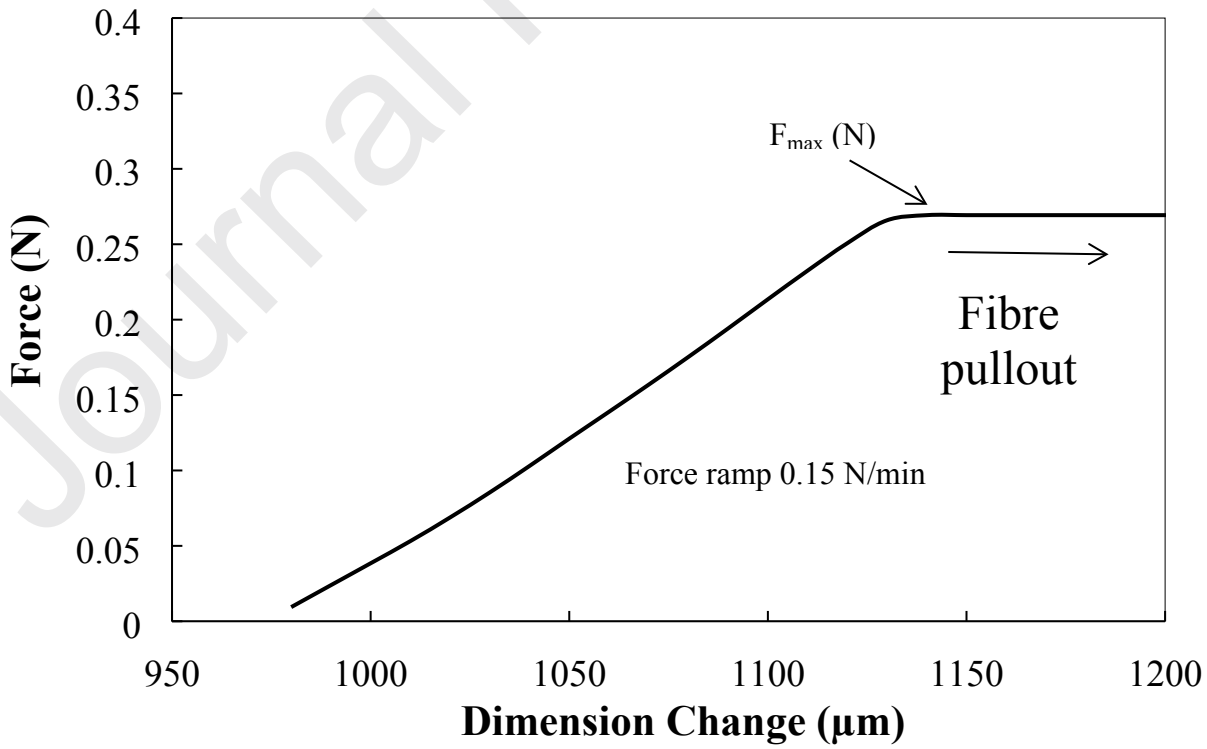

Figure 2. Load/ Displacement Curve for TMA microbond test.

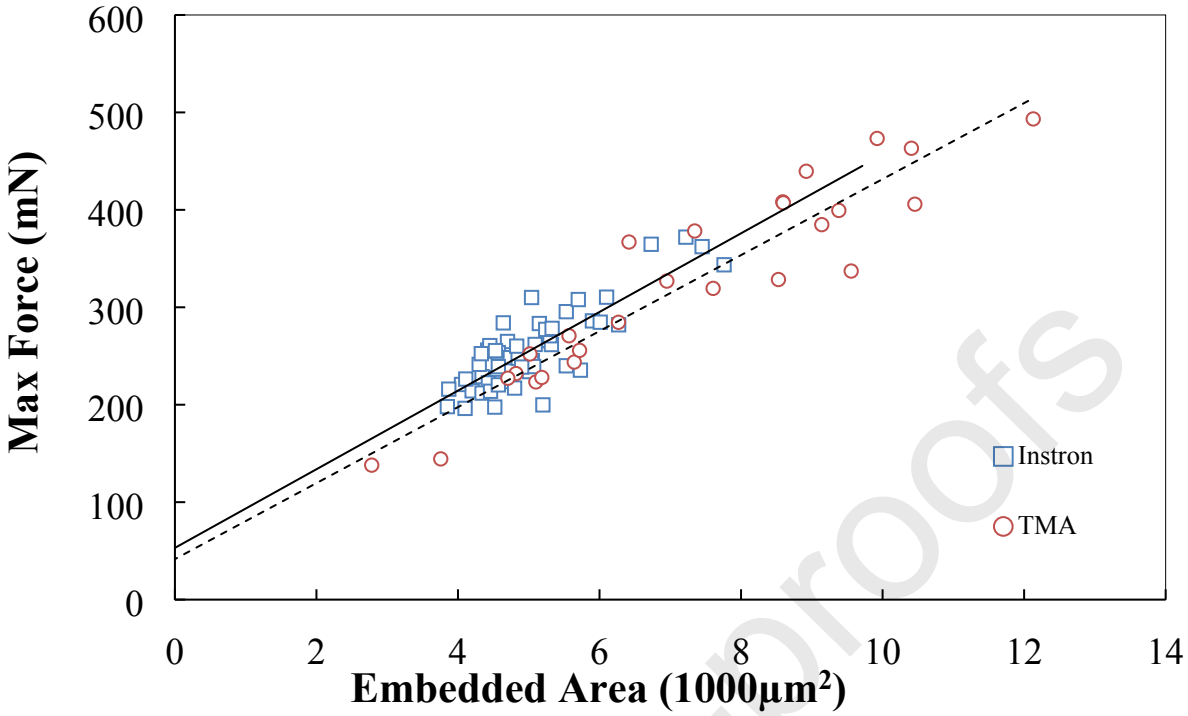

Figure 3. Comparison between force/displacement plots collected using the TMA microbond technique and data collected using the Instron microbond technique, amine (hardener)-to-epoxy (resin) ratio = 1.22 and testing temperature = 20 °C.

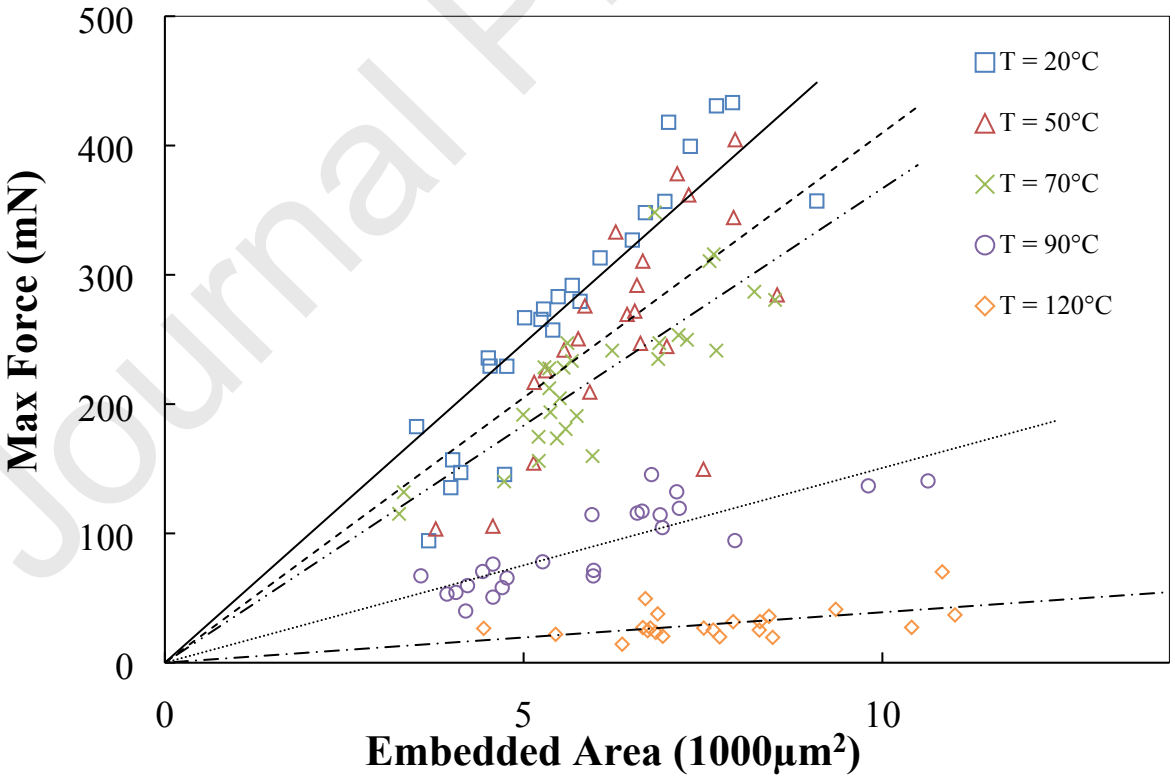

Figure 4. Comparison between force/displacement plots for amine (hardener)-to-epoxy (resin) ratio = 1.04 at different testing temperatures.

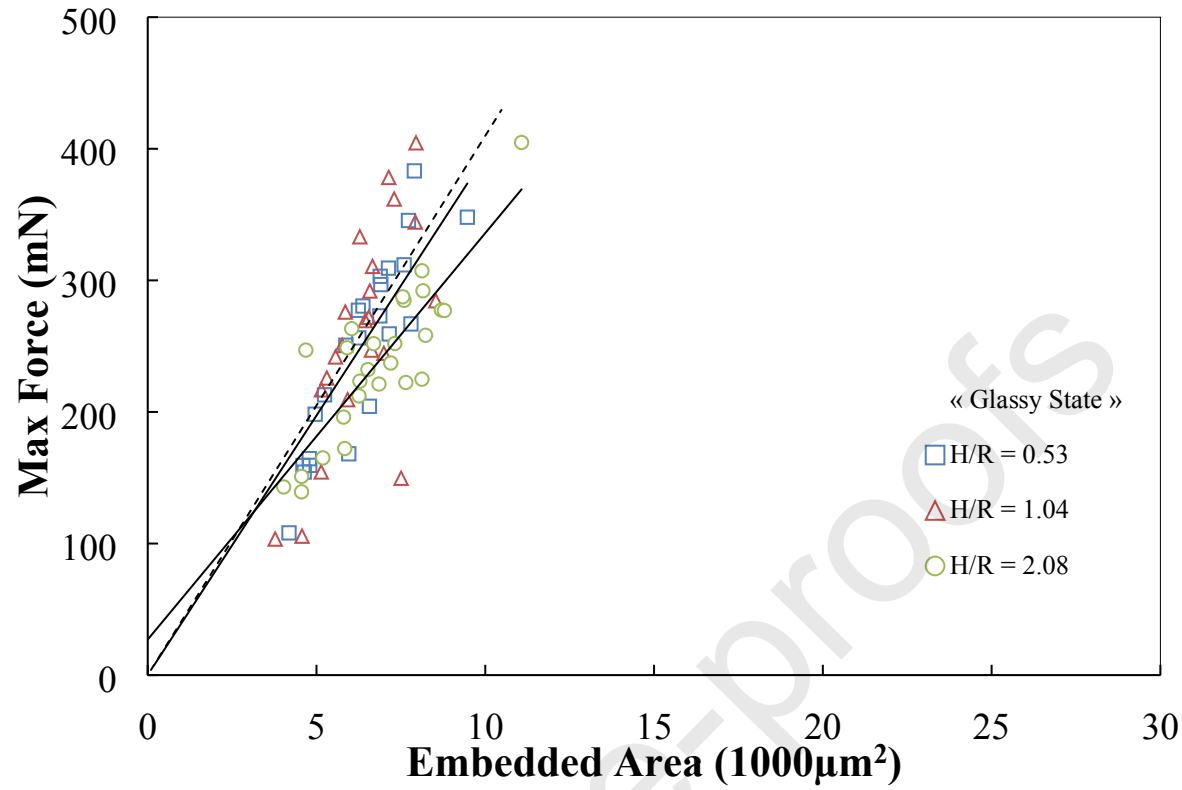

Figure 5. Comparison between force/displacement plots for different amine (hardener)-to-epoxy (resin) ratios at a testing temperature 50 °C.

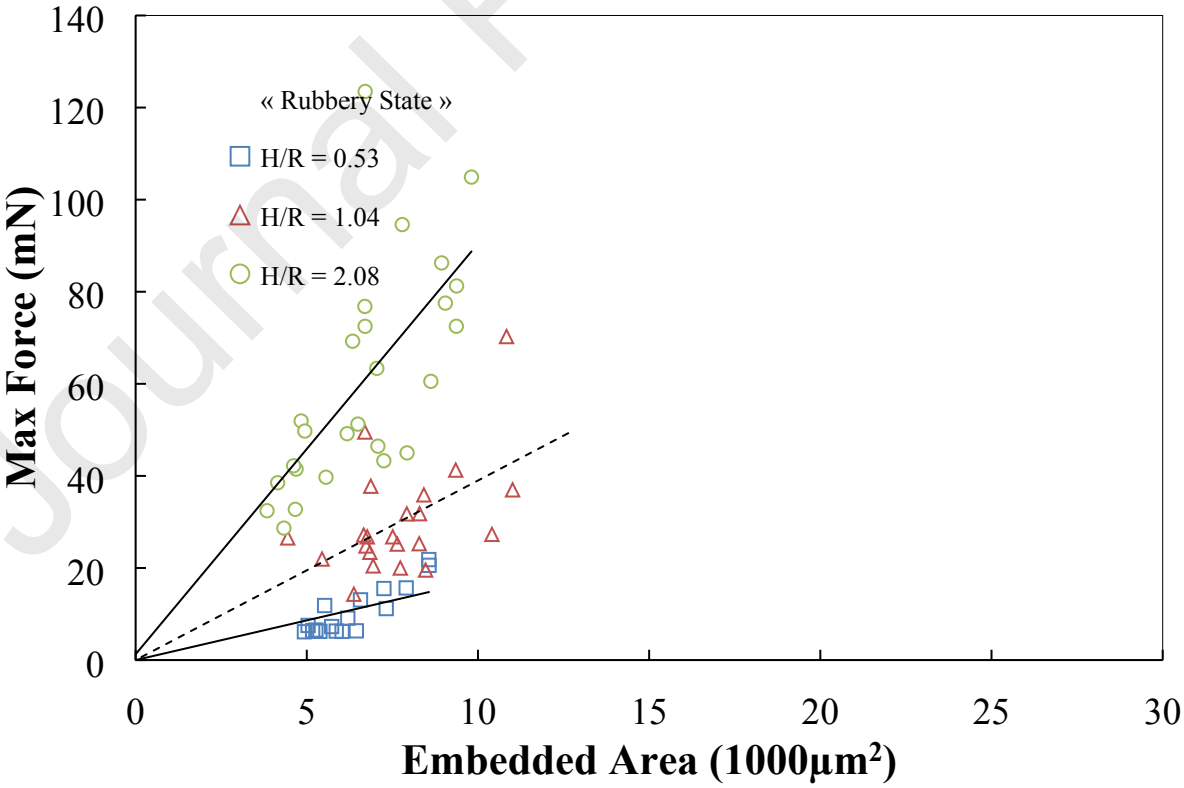

Figure 6. Comparison between force/displacement plots for different amine (hardener)-to-epoxy (resin) ratios at a testing temperature 120 °C.

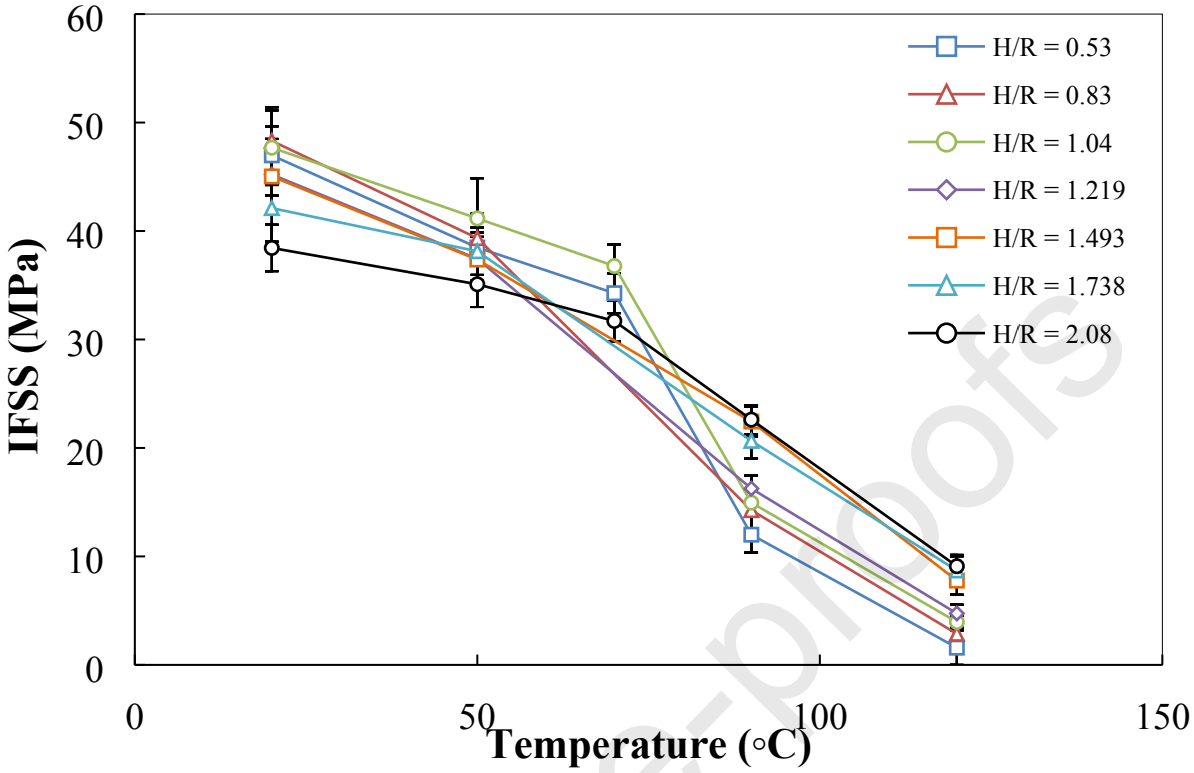

Figure 7. Plot of IFSS versus Testing Temperature for APS fibres.

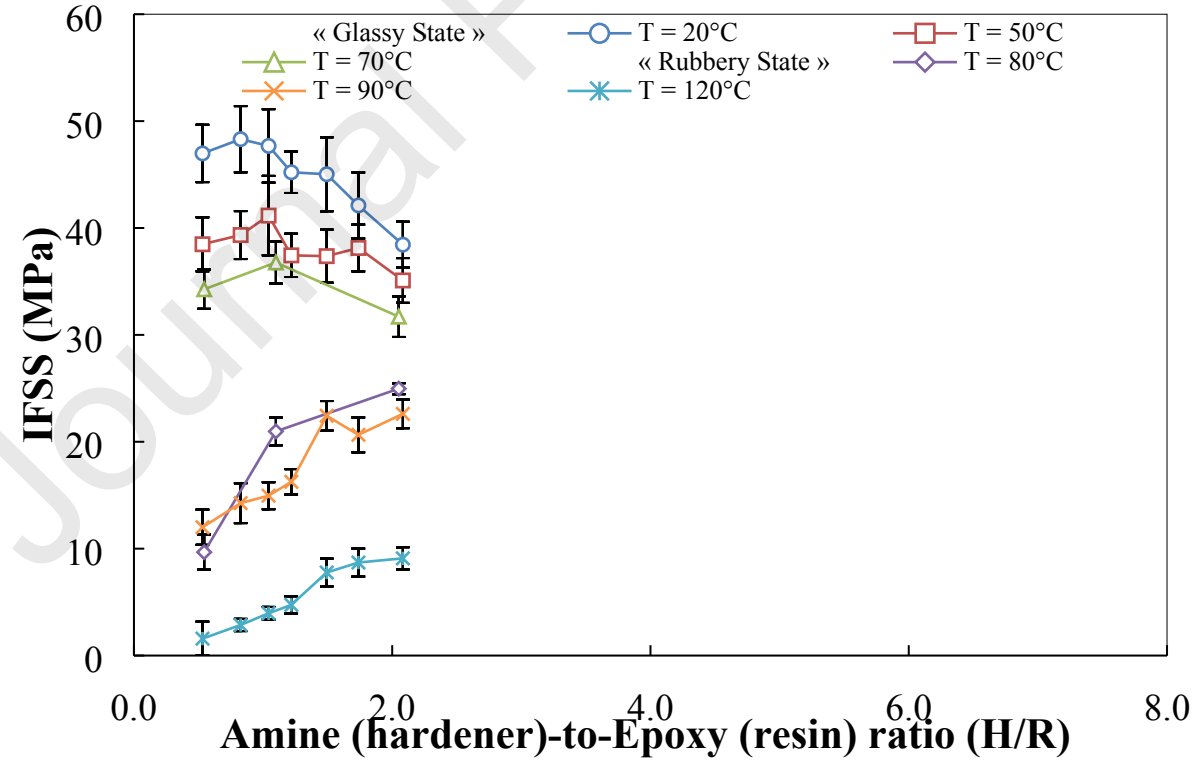

Figure 8. Plot of IFSS versus amine (hardener)-to-epoxy (resin) ratio (H/R) for APS fibres.

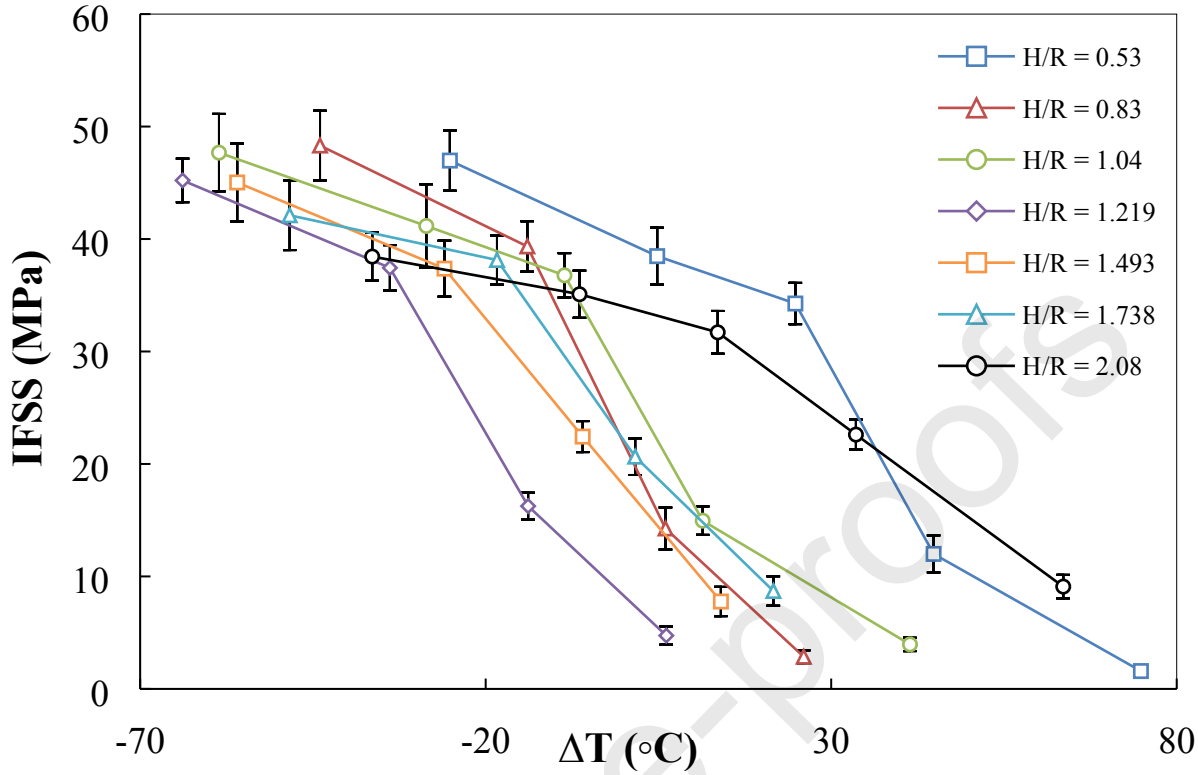

Figure 9. Plot of IFSS versus ΔT, where $\Delta T = T_t - T_g$ for APS fibres.

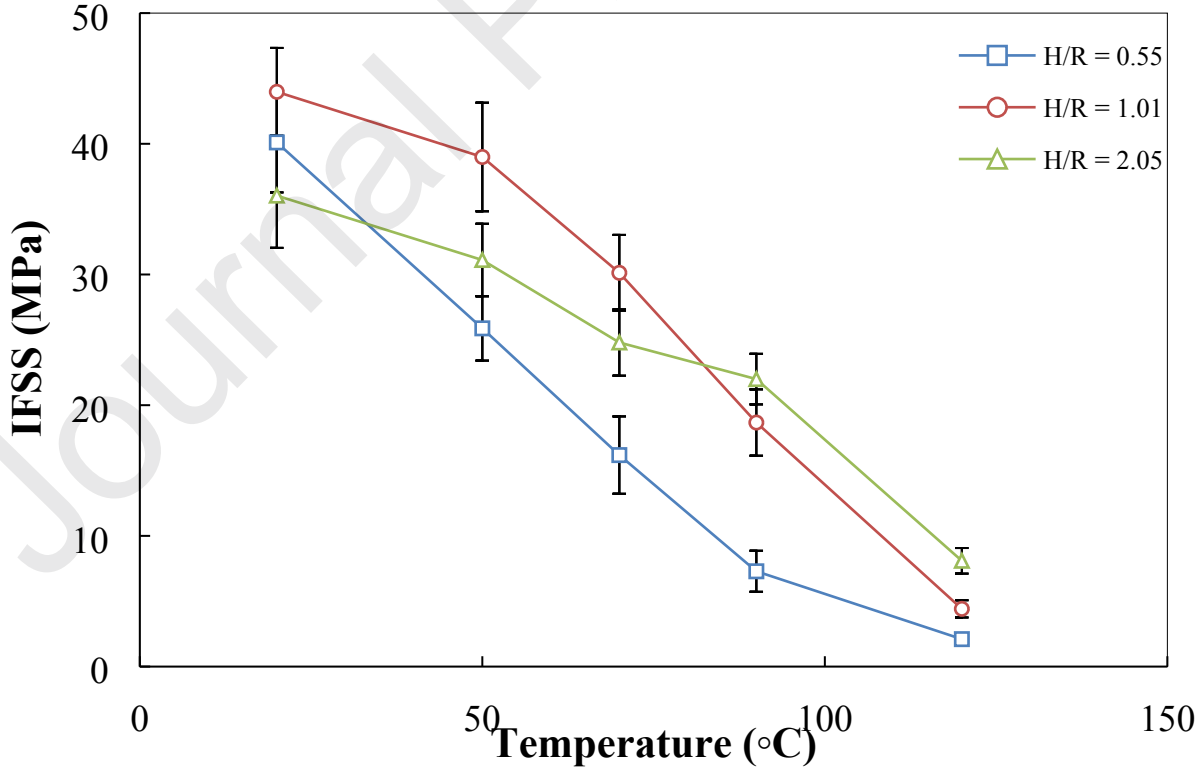

Figure 10. Plot of IFSS versus Testing Temperature for GPS fibres.

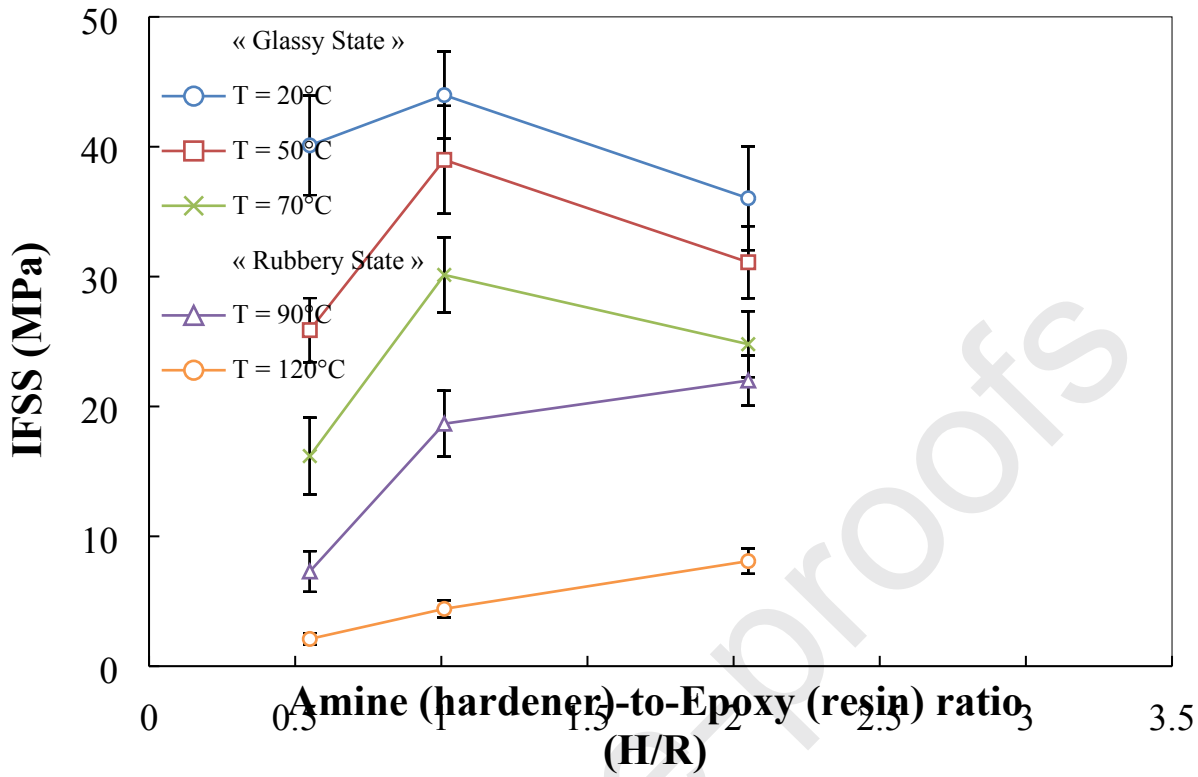

Figure 11. Plot of IFSS versus amine (hardener)-to-epoxy (resin) ratio (H/R) for GPS fibres.

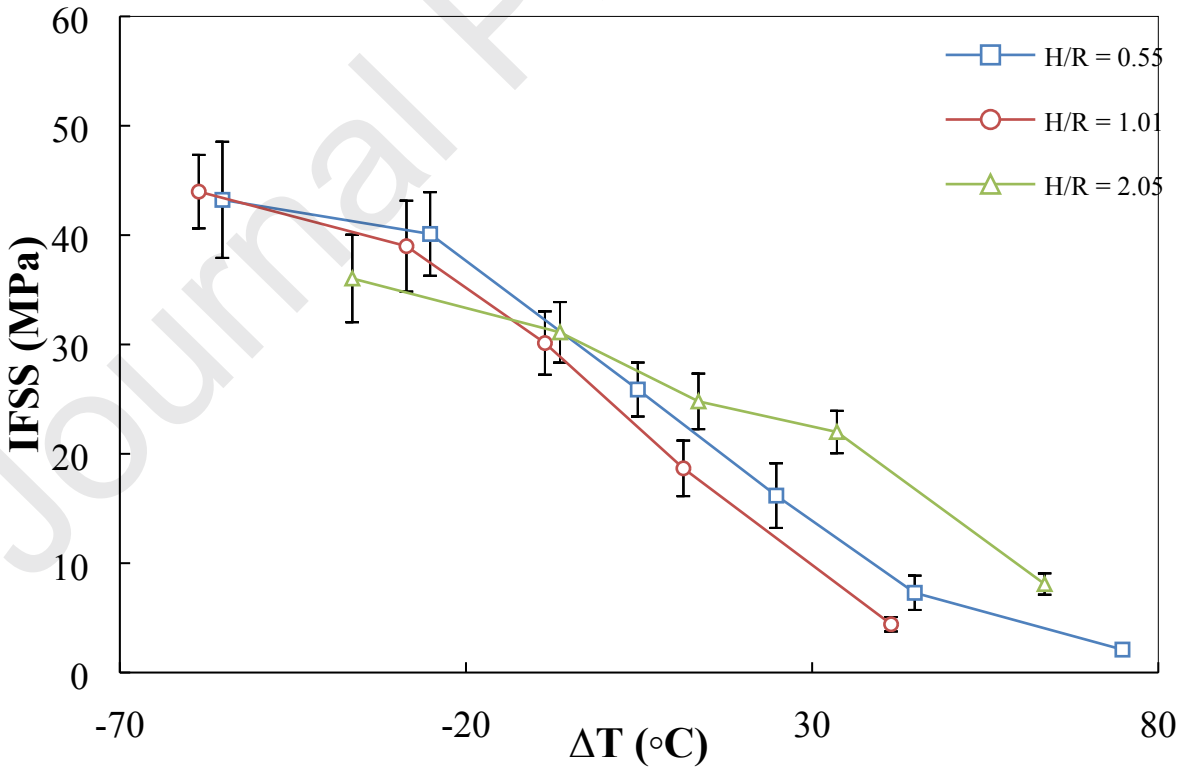

Figure 12. Plot of IFSS versus ΔT, where $\Delta T = T_t - T_g$ for GPS fibres.

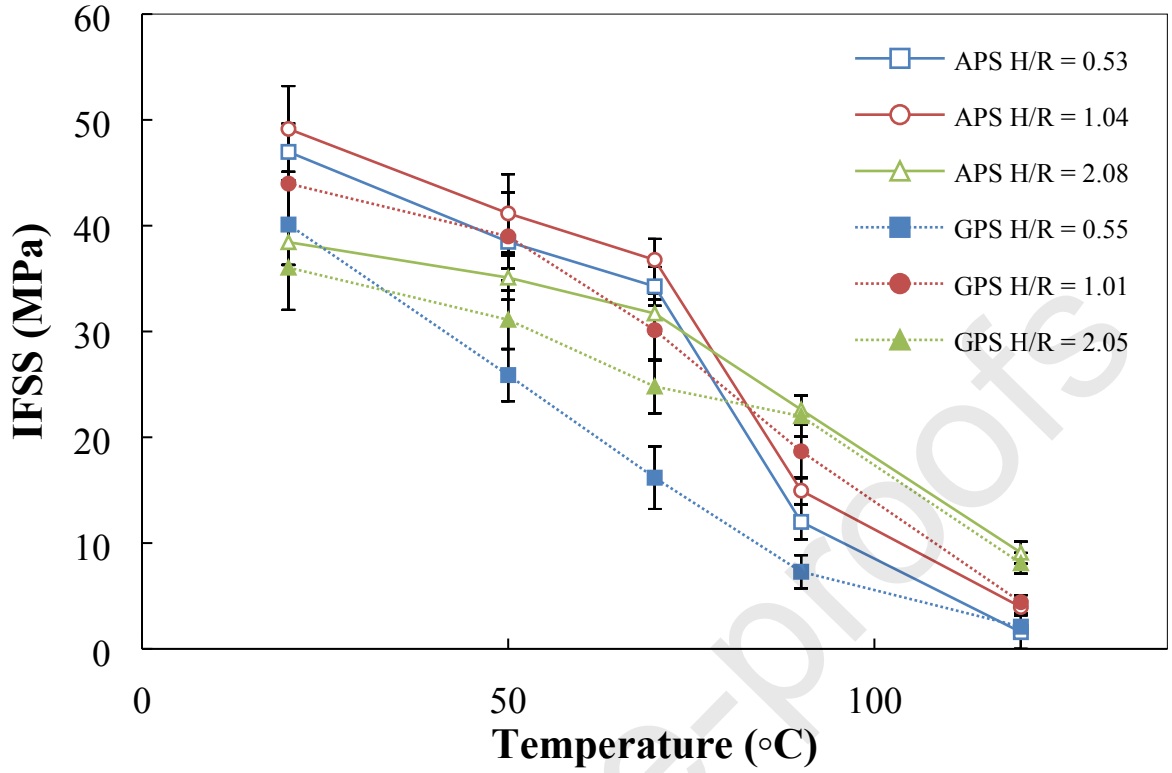

Figure 13. Plot comparing results for H/R ≈ 0.5, H/R ≈ 1.0 and H/R ≈ 2.0 for both silanes studied.

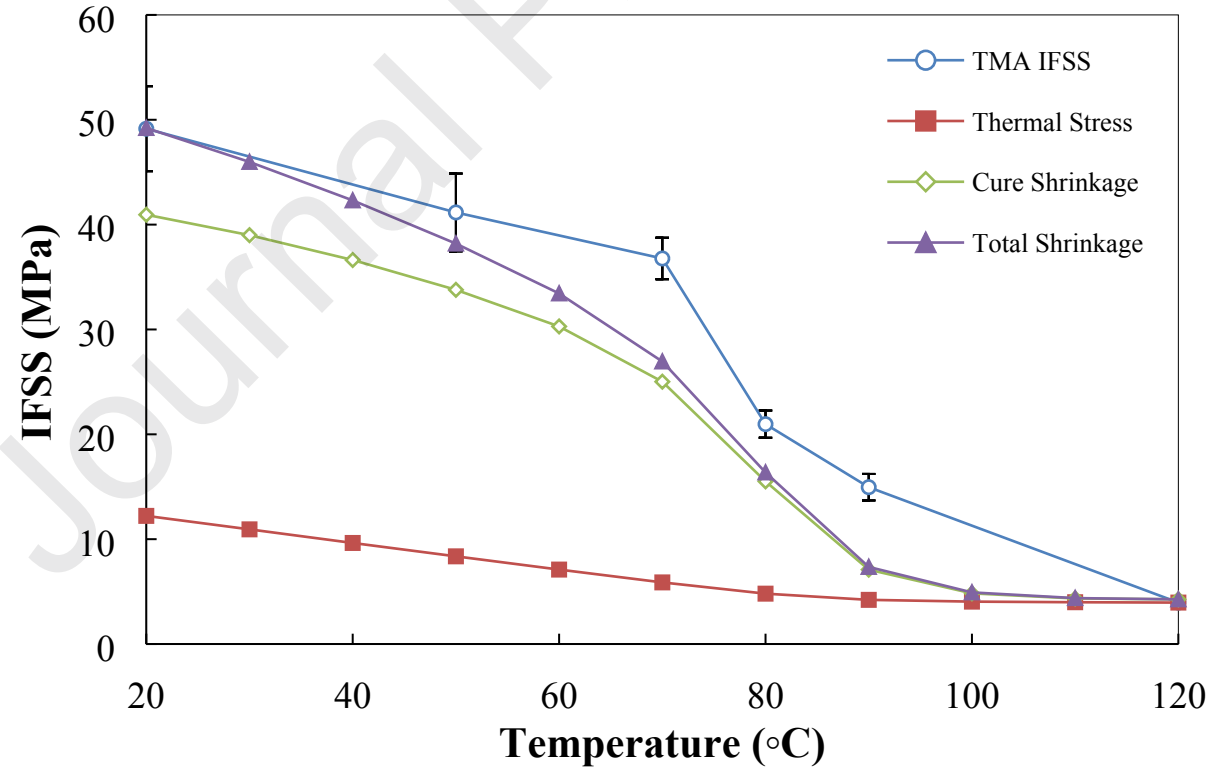

Figure 14. Comparison of glass fibre epoxy IFSS with calculated residual radial stresses for an amine (hardener)-to-epoxy (resin) ratio of H/R ≈ 1.0 (the stoichiometric value).

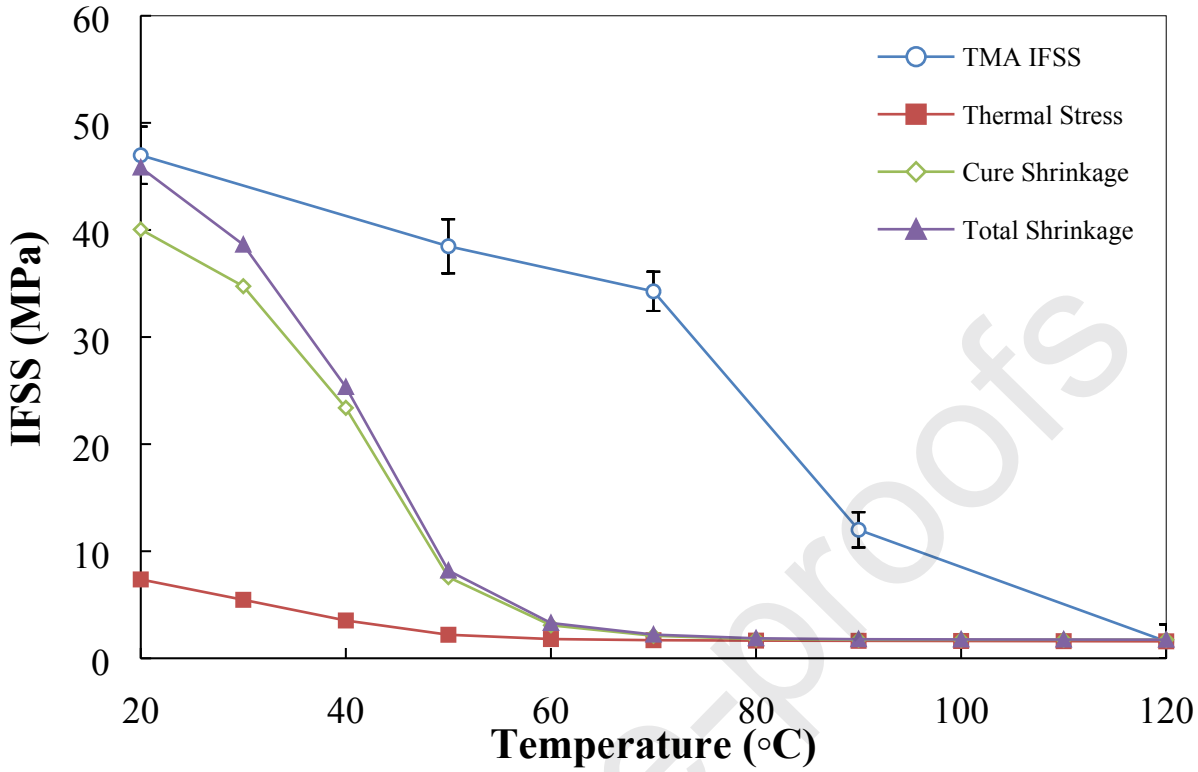

Figure 15. Comparison of glass fibre epoxy IFSS with calculated residual radial stresses for an amine (hardener)-to-epoxy (resin) ratio of H/R ≈ 0.5.

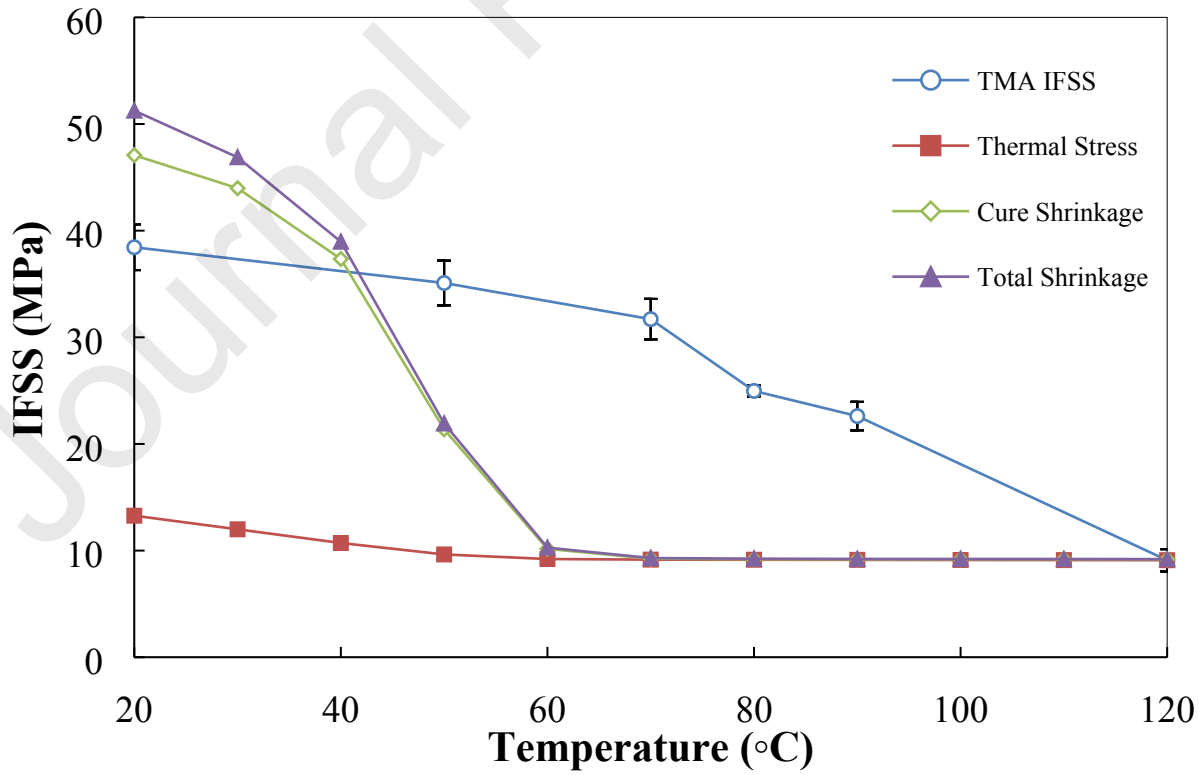

Figure 16. Comparison of glass fibre epoxy IFSS with calculated residual radial stresses for an amine (hardener)-to-epoxy (resin) ratio of H/R ≈ 2.0.

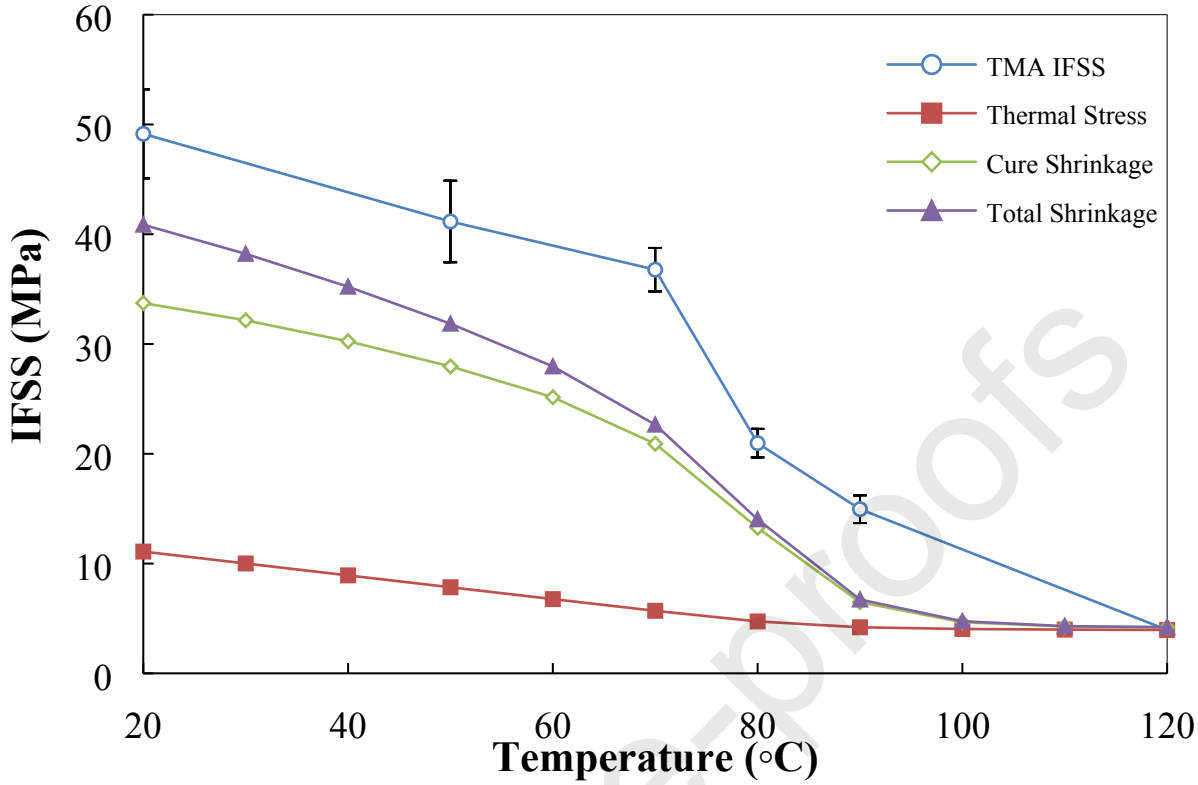

Figure 17. Comparison of glass fibre epoxy IFSS with adjusted residual radial stresses for an amine (hardener)-to-epoxy (resin) ratio of H/R ≈ 1.0 (the stoichiometric value).

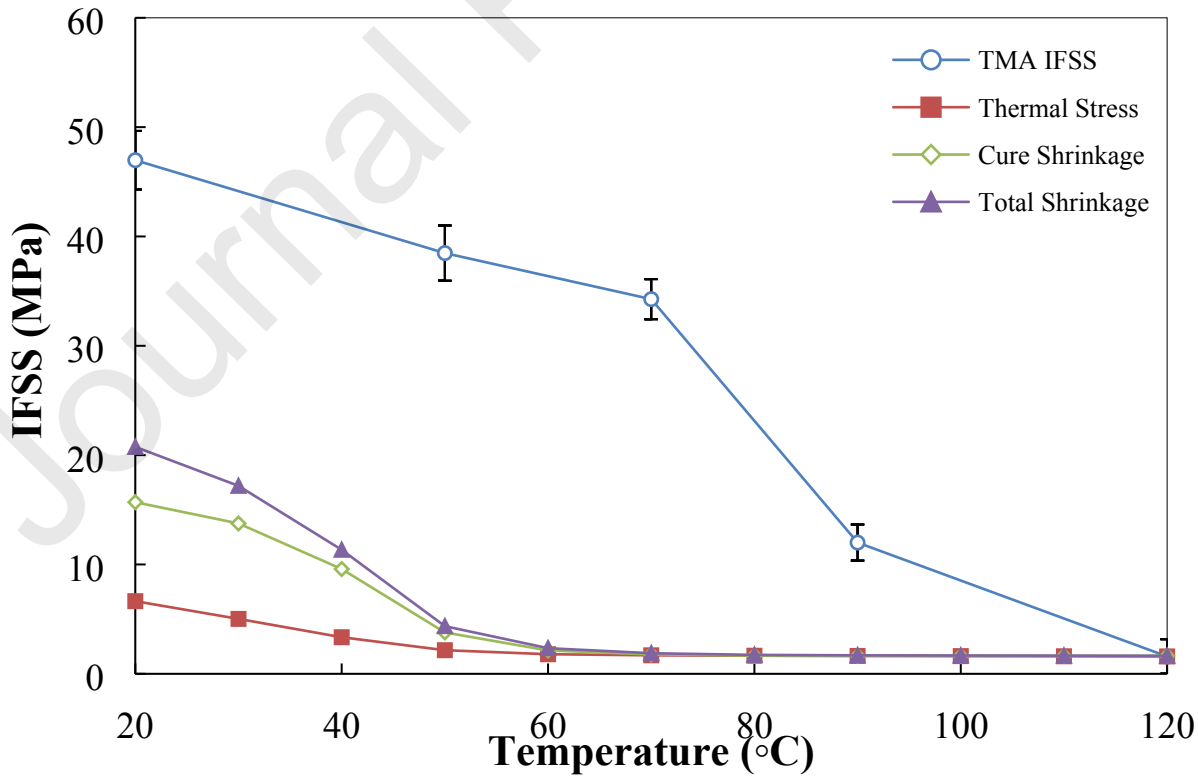

Figure 18. Comparison of glass fibre epoxy IFSS with adjusted residual radial stresses for an amine (hardener)-to-epoxy (resin) ratio of H/R ≈ 0.5.

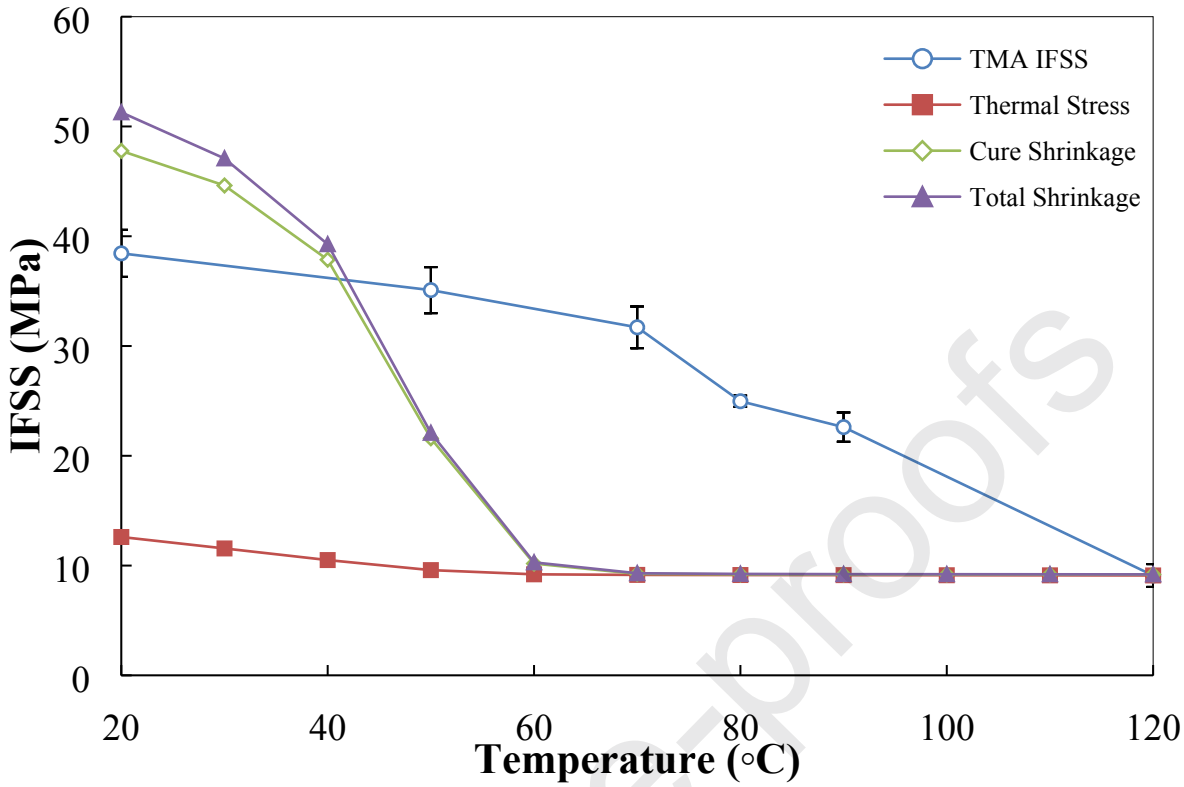

Figure 19. Comparison of glass fibre epoxy IFSS with adjusted residual radial stresses for an amine (hardener)-to-epoxy (resin) ratio of H/R ≈ 2.0.

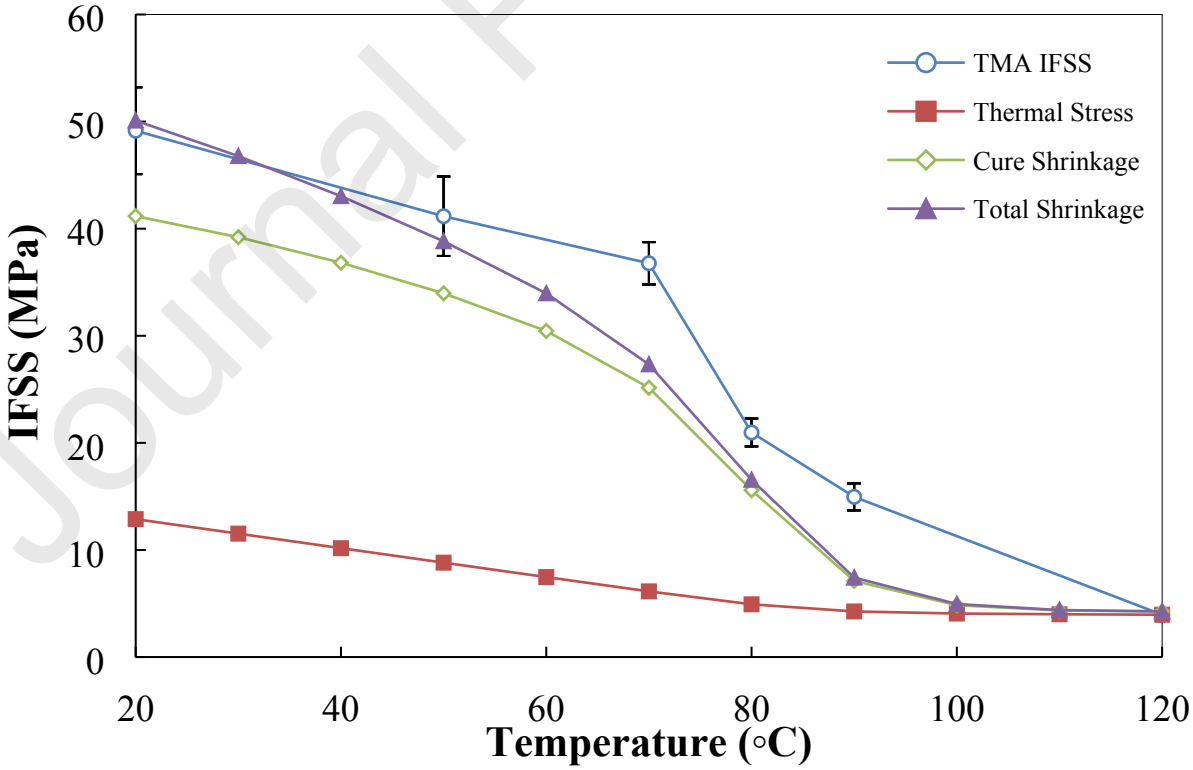

Figure 20. Comparison of glass fibre epoxy IFSS with adjusted residual radial stresses for an amine (hardener)-to-epoxy (resin) ratio of H/R ≈ 1.0 (the stoichiometric value) using a coefficient of static friction = 0.75.

CRediT authorship contribution statement

Ross Minty: Investigation, Data curation, Formal analysis, Writing – original draft, Writing - review & editing. **Liu Yang**: Methodology, Supervision, Writing - review & editing. **James Thomason**: Conceptualization, Funding acquisition, Supervision, Writing - review & editing.

Declaration of interests

☒ The authors declare that they have no known competing financial interests or personal relationships that could have appeared to influence the work reported in this paper.

☐ The authors declare the following financial interests/personal relationships which may be considered as potential competing interests: